Counterpropagating entangled photons from a waveguide with periodic nonlinearity

Mark C. Booth,[1,*] Mete Atatüre,[2] Giovanni Di Giuseppe,[3,‡] Bahaa E. A. Saleh,[3] Alexander V. Sergienko,[2,3] and Malvin C. Teich[1,2,3]

[1]*Quantum Imaging Laboratory,[†] Department of Biomedical Engineering, Boston University, 8 Saint Mary's Street, Boston, Massachusetts 02215*

[2]*Quantum Imaging Laboratory, Department of Physics, Boston University, 8 Saint Mary's Street, Boston, Massachusetts 02215*

[3]*Quantum Imaging Laboratory, Department of Electrical & Computer Engineering, Boston University, 8 Saint Mary's Street, Boston, Massachusetts 02215*

(Received 31 January 2002; published 26 August 2002)

The conditions required for spontaneous parametric down-conversion in a waveguide with periodic nonlinearity in the presence of an unguided pump field are established. Control of the periodic nonlinearity and the physical properties of the waveguide permits the quasiphase matching equations that describe counterpropagating guided signal and idler beams to be satisfied. We compare the tuning curves and spectral properties of such counterpropagating beams to those for copropagating beams under typical experimental conditions. We find that the counterpropagating beams exhibit a narrow bandwidth, permitting the generation of quantum states that possess discrete-frequency entanglement. Such states may be useful for experiments in quantum optics and technologies that benefit from frequency entanglement.

DOI: 10.1103/PhysRevA.66.023815 PACS number(s): 42.65.Ky, 42.65.Wi, 42.79.Gn, 03.65.Ud

I. INTRODUCTION

To achieve successful frequency mixing of optical waves in a nonlinear medium, it is essential that the relative phase between the interacting waves vanish. In the bulk nonlinear media most often encountered in nonlinear optics, *birefringent* phase matching is used to correct for the phase difference [1,2]. The difference in refractive index for each polarization of the interacting waves serves to correct the phase mismatch and ensure effective coupling among the waves. However, this method fails when the medium does not exhibit sufficient birefringence at the interacting wavelengths. As an alternative to birefringent phase matching, waveguide structures can also be utilized to achieve wave coupling [3]. Coupled-mode theory describes the power transfer among guided waves and relies on matching the propagation constants of the interacting fields along the direction of travel, rather than the wave vector for each optical wave. By careful selection of the waveguide dimensions and other properties such as the index profile, the modal structure of the interacting waves can be altered such that efficient frequency mixing can be realized within the waveguide.

Yet another method to correct for phase mismatch is to introduce periodic structure into the nonlinear medium, which results in what is termed *quasiphase matching* (QPM). This approach was independently proposed by Armstrong *et al.* [4] and Franken and Ward [5] in the early 1960s. Of particular interest is a technique for modulating the sign of the second-order nonlinearity throughout the medium to produce a so-called *periodically poled material*. Since any interaction within the transparency region of such a periodically poled material can be noncritically phase matched at a specific temperature via QPM, it is possible to utilize the largest value of the effective nonlinear coefficient for a given material and thus increase the overall conversion efficiency. In the family of commonly used nonlinear media, lithium niobate ($LiNbO_3$) boasts one of the largest nonlinear coefficients d_{33} for all beams having extraordinary polarization; it is approximately six times greater than the d_{31} coefficient used in birefringent phase matching [6]. The result is a theoretical enhancement of $(2d_{33}/\pi d_{31})^2 \sim 20$ for QPM over birefringent phase matching [7]. Many of the advantages of QPM in lithium niobate have been outlined elsewhere [8] and results show that periodically poled lithium niobate (PPLN) is a natural choice for many experiments.

The enhancement in nonlinear-interaction efficiency promised by the use of PPLN has raised interest in the quantum-optics community where there has been a growing interest in new ultrabright sources of entangled photons [9]. Entangled photons, which may be generated through the process of spontaneous parametric down-conversion (SPDC) in a crystal with $\chi^{(2)}$ nonlinearity, has long been in the spotlight for quantum-optics experiments [10,11]. SPDC, however, suffers from low conversion efficiency, on the order of 10^{-9} entangled-photon pairs per mode per pump photon, which ultimately limits its use in many practical applications. Lithium niobate offers the promise of increased photon-pair production and, with the integration of a waveguide structure, control of the spatial characteristics of the down-converted photons while still maintaining a substantial increase in conversion efficiency [9,12]. Since the interaction volume in a waveguide is typically smaller than that in a bulk crystal, it might be thought that this would result in reduced conversion efficiency. However, if comparable pump power is delivered into the waveguide, the photon-pair flux would be identical to that in the bulk crystal for the same $\chi^{(2)}$ nonlinearity.

It turns out, however, that the use of a waveguide struc-

*Electronic address: mbooth@bu.edu

†Quantum Imaging Laboratory URL: http://www.bu.edu/qil

‡Also at Istituto Elettrotecnico Nazionale "G. Ferraris," Strada delle Cacce 91, I-10153 Torino, Italy.

ture, in conjunction with periodic poling, offers yet another critically important feature: the possibility of generating counterpropagating signal and idler photons. Counterpropagation has been previously considered in the context of surface birefringence in nanostructure semiconductors [13].

In this paper, we consider the conditions required for generating counterpropagating photon beams by quasiphase matching in waveguides with periodic nonlinearity and we explore the unique properties of this source of light. Such a source of entangled photons would be immediately useful in quantum-interference experiments that make use of spatial filters [14]. Such filters are often used to restore visibility in these kinds of experiments but they carry the price of a significant reduction in the photon-pair rate.

II. SPDC IN A SINGLE-MODE WAVEGUIDE

By virtue of a relatively weak interaction, time-dependent perturbation theory leads to a two-photon state generated by SPDC at the crystal output that is given by [15]

$$|\Psi^{(2)}\rangle \sim \int_V dV \int dt \chi^{(2)}(z) \hat{E}_{\mathrm{p}}^{(+)}(\mathbf{r},t) \hat{E}_{\mathrm{s}}^{(-)}(\mathbf{r},t) \hat{E}_{\mathrm{i}}^{(-)}(\mathbf{r},t)|0\rangle, \tag{1}$$

where V is the interaction volume, $\chi^{(2)}$ is the second-order susceptibility of the medium, $\mathbf{r}$ is the position vector, and $\hat{E}_j^{(\pm)}$ is the positive- or negative-frequency part of the pump, signal, or idler electric-field operator ($j=\mathrm{p,s,i}$), respectively. In a waveguide, the single-mode signal and idler fields can be described by

$$\hat{E}_j^{(-)}(\mathbf{r},t) = \int d\omega_j u_0(\mathbf{x};\omega_j) e^{-i\beta_j z} e^{i\omega_j t} \hat{a}_j^{\dagger}(\omega_j,\beta_j), \tag{2}$$

where u_0 corresponds to the fundamental mode of the waveguide, $\mathbf{x}$ is the transverse position vector, $\beta_j = \beta_j(\omega)$ are the propagation constants, and $\hat{a}_j^{\dagger}$ are the creation operators, with $j=\mathrm{s,i}$, respectively. As long as the propagation constants for signal and idler fields, β_{s} and β_{i}, are larger than a critical propagation constant β_{c}, determined by the waveguide properties, there is only one fundamental mode available for the propagation of each of the signal and idler fields. If such a condition is met for both the signal and idler fields, then this corresponds to a single-mode waveguide for these fields, as illustrated in Fig. 1 for an arbitrary pump field. This assumption is retained throughout the remainder of this paper.

If it is assumed, furthermore, that the complex pump field is classical,

$$E_{\mathrm{p}}(\mathbf{r},t) = \int d\omega_{\mathrm{p}} \mathcal{E}_{\mathrm{p}}(\mathbf{x};\omega_{\mathrm{p}}) e^{i\beta_{\mathrm{p}} z} e^{-i\omega_{\mathrm{p}} t}, \tag{3}$$

where $\mathcal{E}_{\mathrm{p}}$ is the transverse and spectral profile of the pump wave, Eqs. (1)–(3) then lead to a two-photon quantum state given by

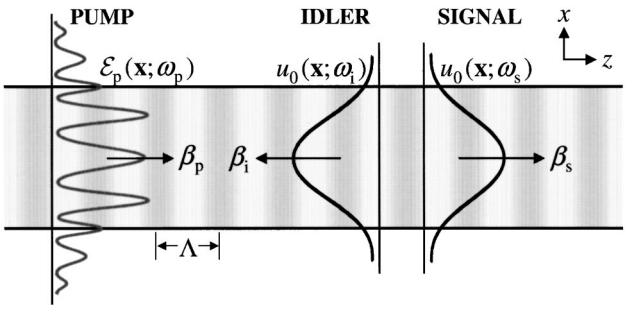

FIG. 1. Schematic of a slab waveguide structure with modulated nonlinearity (illustrated as striations). The pump has an arbitrary spatial profile whereas the signal and idler beams are assumed to occupy the fundamental TE electric-field modes of the waveguide.

$$\begin{aligned}|\Psi^{(2)}\rangle \sim \int_A d\mathbf{x} dz \int dt \int d\omega_{\mathrm{p}} d\omega_{\mathrm{s}} d\omega_{\mathrm{i}} \mathcal{E}_{\mathrm{p}}(\mathbf{x};\omega_{\mathrm{p}}) \\ \times u_0(\mathbf{x};\omega_{\mathrm{s}}) u_0(\mathbf{x};\omega_{\mathrm{i}}) \chi^{(2)}(z) e^{i\Delta\beta z} \\ \times e^{-i(\omega_{\mathrm{p}}-\omega_{\mathrm{s}}-\omega_{\mathrm{i}})t} \hat{a}_{\mathrm{s}}^{\dagger}(\omega_{\mathrm{s}},\beta_{\mathrm{s}}) \hat{a}_{\mathrm{i}}^{\dagger}(\omega_{\mathrm{i}},\beta_{\mathrm{i}})|0\rangle,\end{aligned} \tag{4}$$

where A is the transverse plane spanned by the vector $\mathbf{x}$ and where

$$\Delta\beta = \beta_{\mathrm{p}} - \beta_{\mathrm{s}} - \beta_{\mathrm{i}} \tag{5}$$

is the phase mismatch between the three fields that must vanish for perfect phase matching.

We can further simplify Eq. (4) by carrying out the integration over t. This yields the condition

$$\omega_{\mathrm{p}} - \omega_{\mathrm{s}} - \omega_{\mathrm{i}} = 0 \tag{6}$$

and, using the Fourier-transform definition

$$\tilde{\chi}^{(2)}(\Delta\beta) = \int dz e^{iz\Delta\beta} \chi^{(2)}(z), \tag{7}$$

we obtain

$$\begin{aligned}|\Psi^{(2)}\rangle \sim \int d\mathbf{x} \int d\omega_{\mathrm{s}} d\omega_{\mathrm{i}} \mathcal{E}_{\mathrm{p}}(\mathbf{x};\omega_{\mathrm{s}}+\omega_{\mathrm{i}}) u_0(\mathbf{x};\omega_{\mathrm{s}}) u_0(\mathbf{x};\omega_{\mathrm{i}}) \\ \times \tilde{\chi}^{(2)}(\Delta\beta) \hat{a}_{\mathrm{s}}^{\dagger}(\omega_{\mathrm{s}},\beta_{\mathrm{s}}) \hat{a}_{\mathrm{i}}^{\dagger}(\omega_{\mathrm{i}},\beta_{\mathrm{i}})|0\rangle\end{aligned} \tag{8}$$

for the two-photon state describing down-converted light in a single-mode waveguide structure.

Finally, applying the creation operators to the vacuum yields

$$|\Psi^{(2)}\rangle \sim \int d\omega_{\mathrm{s}} d\omega_{\mathrm{i}} \Phi(\omega_{\mathrm{s}},\omega_{\mathrm{i}})|1\rangle_{\omega_{\mathrm{s}}}|1\rangle_{\omega_{\mathrm{i}}}, \tag{9}$$

with a state function Φ [16] given by

$$\Phi(\omega_{\mathrm{s}},\omega_{\mathrm{i}}) = \int_A d\mathbf{x} \mathcal{E}_{\mathrm{p}}(\mathbf{x};\omega_{\mathrm{s}}+\omega_{\mathrm{i}}) u_0(\mathbf{x};\omega_{\mathrm{s}}) u_0(\mathbf{x};\omega_{\mathrm{i}}) \tilde{\chi}^{(2)}(\Delta\beta). \tag{10}$$

The ket $|1\rangle_{\omega_s}|1\rangle_{\omega_i}$ represents a single photon in the frequency mode ω_s and a single photon in the frequency mode ω_i with corresponding propagation constants β_s and β_i, respectively. Since the down-converted light is guided in only a single spatial mode, the magnitude squared of the state function, $|\Phi(\omega_s,\omega_i)|^2$, represents the spectrum of the SPDC, which will be considered subsequently.

The theory presented to this point is general and can be applied to any structure with an arbitrary nonlinearity profile. In this paper, we focus on a second-order susceptibility that is periodically modulated in the z direction, so that $\chi^{(2)}(z)$ can be written as a Fourier series and takes the form

$$\chi^{(2)}(z)=\chi_0^{(2)}\sum_m G_m e^{iK_m z}. \tag{11}$$

Here m corresponds to the mth component of the Fourier expansion with coefficient G_m and wave number $K_m = 2\pi m/\Lambda$, where Λ is the periodicity of the modulation. Since the phase mismatch $\Delta\beta$ among the propagation constants of the three fields is most often not zero, we must use the contribution K_m, associated with the modulation of the nonlinearity in the material, to achieve perfect quasiphase matching in the waveguide [$\Delta\beta = K_m$ in Eq. (5)]. We may therefore define a phase mismatch $\Delta\beta'$ in the presence of the grating vector K_m given by

$$\Delta\beta' = \beta_p - \beta_s - \beta_i - K_m. \tag{12}$$

When $\Delta\beta' = 0$, this is referred to as perfect quasiphase matching.

For a nonlinearity with a single periodicity, $K_{\pm m} = \pm K_m$ so that negative values of m may also yield meaningful solutions to the QPM conditions given in Eq. (12). In conjunction with the multiple signal-idler wavelength combinations generated with SPDC, contributions from both positive and negative values of m can be simultaneously realized. This is in contradistinction to three-wave mixing problems such as second-harmonic generation [8], where the two input fields are fixed and yield only one output field. In this latter case, the grating vector corresponding to the negative value of m is not utilized since it does not yield a simultaneous phase-matching solution.

III. COUNTERPROPAGATING SPDC IN A PPLN WAVEGUIDE

We continue our analysis by considering the specific example of a PPLN waveguide and proceed to describe some interesting properties of single-mode, counterpropagating signal and idler beams, under various conditions.

Without loss of generality, we consider a waveguide in two dimensions [17]: x as the transverse (guiding) dimension and z as the longitudinal (propagating) dimension. We further assume that the pump field in Eq. (3) is a monochromatic unguided and undepleted plane wave with a transverse spatial profile given by

$$\mathcal{E}_p(x;\omega_p) = A_p \cos[(k_p \sin\theta)x], \tag{13}$$

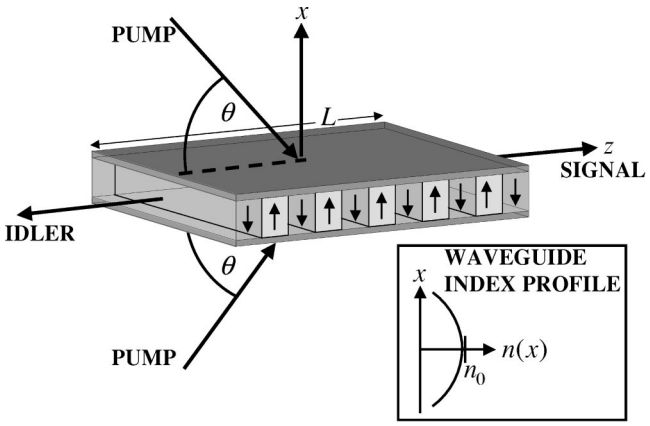

FIG. 2. Schematic of a PPLN slab waveguide with the plane-wave pump beams incident at the angles of incidence $\pm\theta$. The pump is unguided whereas the counterpropagating signal and idler beams are assumed to populate the fundamental mode of the waveguide. The medium comprising the waveguide is taken to have a parabolic index profile $n(x)$ as shown in the inset and to have a nonlinear susceptibility $\chi^{(2)}(z)$ that has a single period. The illustration shows a square-wave modulation of $\chi^{(2)}$; the arrows indicate regions of positive and negative values of the nonlinear coefficient.

where A_p is a constant and k_p is the pump wave number. Such a field can be realized by illuminating the waveguide with two identical coherent fields at angles $\pm\theta$ from the z axis. An illustration of a planar dielectric waveguide structure pumped in this geometry is shown in Fig. 2. Since the power of the pump beam can be increased to any desired level, loss of pump beam energy is not critical for effective operation. Our example of an unguided pump beam is distinct from a scheme for copropagating difference frequency generation, in which both the pump beam and signal photon are guided and a copropagating idler photon is allowed to radiate into the substrate [6].

To compute tuning curves from Eq. (6) and Eq. (12), where the pump beam is incident on the waveguide structure at an angle θ, we use $\beta_p = k_p \cos\theta$. We allow the propagation constant β_i for the idler field to take on a negative value to permit counterpropagation. Finally, to compute the specific values of β_j for each field, we use the set of Sellmeier equations for lithium niobate [18] to determine the refractive index for extraordinarily polarized (e) waves in the e$\rightarrow$e+e interaction under consideration. Although Eq. (12) only describes perfect phase matching ($\Delta\beta' = 0$), we are nonetheless able to determine many interesting properties of counterpropagating signal and idler photons. These are presented as tuning curves, representing various properties of the down-converted light as a function of the pump-beam incidence angle.

To investigate the relationship of the poling period and the pump-beam incidence angle for quasiphase matching, we first consider only the degenerate case where the pump field gives rise to counterpropagating signal and idler photons at twice the pump wavelength ($\lambda_s = \lambda_i = 2\lambda_p = 1064$ nm). Figure 3 shows the required poling period Λ that allows for perfect QPM at any pump-beam incidence angle. Immediately evident from this plot is that, for a pump beam that is

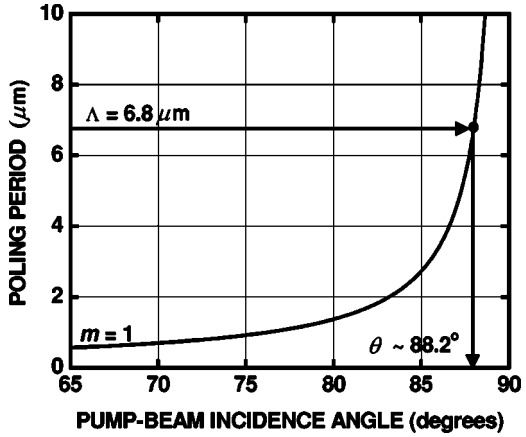

FIG. 3. Degenerate tuning curve for perfect QPM ($\Delta\beta'=0$): Poling period Λ ($m=1$) vs pump-beam incidence angle θ for degenerate down-conversion in a PPLN waveguide with counterpropagating signal and idler photons at $\lambda_s=\lambda_i=1064$ nm. The pump wavelength $\lambda_p=532$ nm.

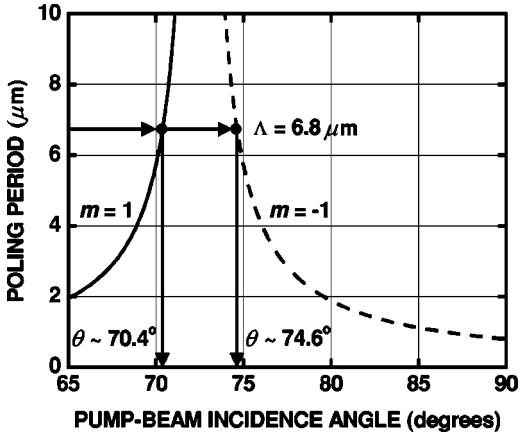

FIG. 4. Nondegenerate tuning curve for perfect QPM ($\Delta\beta'=0$): Poling period Λ ($m=\pm1$) vs pump-beam incidence angle θ for nondegenerate down-conversion in a PPLN waveguide with counterpropagating signal and idler photons at $\lambda_s=810$ nm and $\lambda_i=1550$ nm. The pump wavelength $\lambda_p=532$ nm.

coupled into the PPLN waveguide at 65°, one would require a poling period on the order of the pump wavelength (0.5 μm). This observation remains true for pump-beam incidence angles less than 65°, including the case for normal incidence at 0°. Since the smallest poling period experimentally achievable with lithium niobate is currently ~ 4 μm [19], this configuration is not currently realizable.

To experimentally realize phase matching for counterpropagating fields in an optical parametric oscillator or amplifier (OPO, OPA) at angles near normal incidence, researchers have been forced to utilize materials such as gallium arsenide, in which it is possible to construct submicrometer multilayer or asymmetric quantum-well domain structures using semiconductor growth techniques. The second-order susceptibility can then be spatially modulated between contiguous layers at the dimension required to successfully achieve phase matching. By varying the pump-beam angle in such devices, QPM may be realized over large tuning ranges in OPOs and OPAs [20].

The use of an unguided pump avoids the necessity for submicrometer poling periods to achieve counterpropagation in PPLN waveguides. To illustrate this, consider the particular first-order poling period $\Lambda=6.8$ μm that corresponds to second-harmonic generation at 532 nm and, therefore, degenerate down-conversion to 1064 nm. For this poling period, we find from Fig. 3 that if we pump the waveguide at an angle of $\sim 88.2°$ we can generate counterpropagating signal and idler beams. When the pump beam is at 90°, $\Lambda \rightarrow \infty$ ($K_m \rightarrow 0$) so that QPM is no longer required for down-conversion and a birefringent interaction will result in counterpropagating signal and idler photons [8].

Most interesting is nondegenerate down-conversion where we select, as a particular example, the signal-idler combination of 810 nm and 1550 nm, respectively. From the tuning curves in Fig. 4 we find that for the same poling period considered in Fig. 3, $\Lambda=6.8$ μm, one can satisfy QPM at two pump angles, namely, $\sim 70.4°$ and $\sim 74.6°$, as a result of the dual directionality of the grating vector K_m. Since there are two angles that satisfy QPM for nondegenerate down-conversion, we expect that for a single angle the dual directionality of the grating vector would allow for different nondegenerate wavelength combinations. In Fig. 5(a), all possible signal-idler wavelength combinations are plotted as the pump-beam incidence angle is varied from 65° to 90°. For this plot, the poling period is fixed at $\Lambda=6.8$ μm and the corresponding tuning curves are plotted for grating vector values with order $m=0,\pm1,\pm2$, and ±3. The selection of tuning curves for experimental implementation is dependent on the nature of the periodicity of the nonlinearity and on the strength of the coefficients G_m in Eq. (11).

As an example, a $\chi^{(2)}$ that is modulated as a square wave in the z direction, as illustrated in Fig. 2, has dominant Fourier components of order ±1, for which tuning curves are shown in Fig. 5(b). If we consider an example where the pump beam angle is 80°, there are signal-idler wavelength combinations of approximately 880 nm/1350 nm ($m=-1$, dashed curve, open circles) and 930 nm/1240 nm ($m=+1$, solid curve, solid circles). This quantum state can be represented by

$$|\Psi^{(2)}\rangle \sim c_1|880,1350\rangle + c_2|930,1240\rangle, \qquad (14)$$

where the constants c_1 and c_2 are determined mainly by the pump properties. By simply selecting the pump-beam incidence angle to be 74.6°, for example, the two-photon quantum state given above can be readily tuned to new signal-idler wavelength combinations of 810 nm/1550 nm and 860 nm/1380 nm.

The generation of a superposition of two counterpropagating nondegenerate photons pairs occurs naturally within the PPLN waveguide structure and this is an interesting property as it stands. Beyond changing the pump-beam incidence angle, control over the down-converted light is further afforded by adjusting the poling period. As the poling period is reduced, the difference between the two signal wavelengths and the two idler wavelengths turns out to increase, i.e., the curves separate from one another. As one increases the pol-

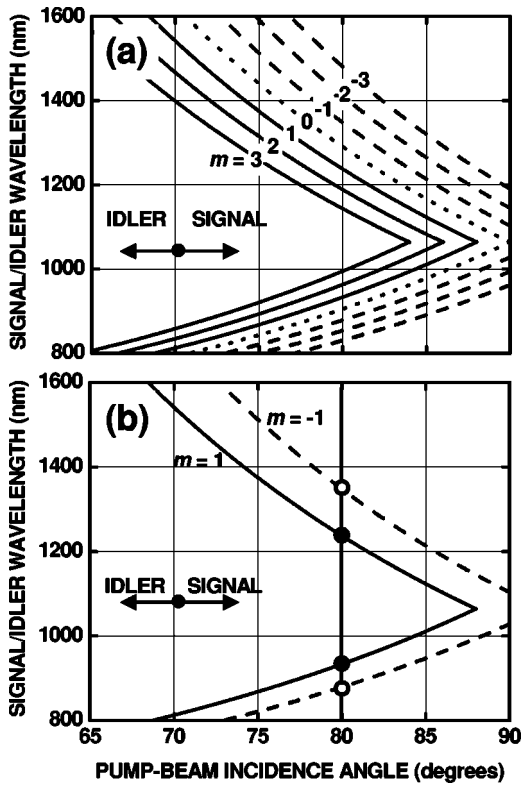

FIG. 5. Tuning curves for perfect QPM ($\Delta\beta'=0$) with various values of m. (a) Signal and idler wavelengths vs pump-beam incidence angle θ for grating vector orders $m=0,\pm1,\pm2$, and ±3 in a PPLN waveguide with a poling period $\Lambda=6.8$ μm. (b) Subset of tuning curves in (a) for $m=\pm1$ with the poling period $\Lambda=6.8$ μm. The signal photon propagates in the positive z direction and the idler photon counterpropagates in the negative z direction as shown by the inset. The pump wavelength $\lambda_p=532$ nm in both (a) and (b). Positive and negative values of m are indicated by solid and dashed curves, respectively. The case where $m=0$ is indicated by a dotted curve. Circles in (b) indicate the two signal-idler combinations possible for a pump-beam incidence angle of 80°: 880 nm/1350 nm ($m=-1$, dashed curve, open circles) and 930 nm/1240 nm ($m=+1$, solid curve, solid circles). Since these plots only consider the case of perfect QPM, they lack the spectral information of the signal and idler photons, which will be presented in Figure 9 below.

ing period or chooses the longer third-order poling period, the signal photons and idler photons become more similar in wavelength, i.e., the curves approach each other.

IV. SPDC SPECTRUM IN A PPLN WAVEGUIDE

The preceding section considered only the idealized phase-matching conditions provided by Eq. (12). In this section, we consider effects on the spatiotemporal distribution of down-converted light imparted by the finite crystal length and the modal structure of the waveguide. The spectrum of down-conversion at the output of the waveguide is computed from the magnitude squared of the state function given in Eq. (10).

As a specific example, and for convenience of calculation, we consider the TE modes of a planar graded-index (GRIN) slab waveguide as illustrated in Fig. 2, with a parabolic index profile [17] along the transverse x axis given by

$$n^2(x)=n_0^2[1-\alpha^2x^2], \tag{15}$$

where n_0 is the maximum core index and $n_0\alpha^2$ is the rate of change of refractive index with position, $dn(x)/dx$. For this case, the fundamental transverse mode becomes [21]

$$u_0(x;\omega_j)=C\exp\left[-\frac{(\gamma_j x)^2}{2}\right], \tag{16}$$

where C is a constant and where

$$\gamma_j=\left[\frac{n_0\omega_j}{c}\alpha\right]^{1/2},\quad \beta_j=\frac{n_0\omega_j}{c}\left[1-\frac{c}{n_0\omega_j}\alpha\right]^{1/2}. \tag{17}$$

Single-mode operation is achieved when

$$\beta_{s,i}>\beta_c=\frac{n_0\omega_{s,i}}{c}\left[1-\frac{3c}{n_0\omega_j}\alpha\right]^{1/2} \tag{18}$$

and we assume that the down-converted light couples only to the fundamental mode of the parabolic waveguide.

By substituting into Eq. (10) the transverse mode profile given by Eq. (16), the unguided pump field given by Eq. (13), and the first-order periodic nonlinearity found from Eq. (11), we find the following expression for the state function:

$$\begin{aligned}\Phi(\omega_s,\omega_i)=A\sqrt{\frac{\pi}{\gamma_{eff}^2}}e^{-\zeta^2/4\gamma_{eff}^2}&\\ \times\left\{\mathrm{sinc}\left[\left(\Delta\beta+\frac{2\pi}{\Lambda}\right)\frac{L}{2}\right]e^{-i(\Delta\beta+2\pi/\Lambda)L/2}\right.&\\ \left.+\mathrm{sinc}\left[\left(\Delta\beta-\frac{2\pi}{\Lambda}\right)\frac{L}{2}\right]e^{-i(\Delta\beta-2\pi/\Lambda)L/2}\right\},&\end{aligned} \tag{19}$$

where A is a constant, $\zeta=[n_0(\omega_s+\omega_i)/c]\sin\theta$, $\gamma_{eff}^2=(1/2)(\gamma_s^2+\gamma_i^2)$, $\mathrm{sinc}x\equiv(\sin x)/x$, and L is the crystal length. Effectively, the SPDC bandwidth is modulated by the prefactor $[\pi/(\gamma_s^2+\gamma_i^2)]^{1/2}\exp(-\zeta^2/4\gamma_{eff}^2)$ associated with the waveguide and will therefore differ from that for bulk media. The spectral profile of the photon pairs can therefore be altered by the waveguide parameters. For the waveguide parameters in the parabolic index-profile example presented here, however, the value of this prefactor remains nearly constant over the computed bandwidth, so that waveguide effects can be ignored, at least for the fundamental mode. If the waveguide operating conditions admit multiple modes, however, the SPDC bandwidth may be more sensitive to the waveguide properties.

We now consider the SPDC bandwidth, measured as the full width at half maximum (FWHM) of the SPDC spectrum obtained from the magnitude squared of Eq. (19), for several interesting configurations in a PPLN waveguide. Figure 6 presents a set of plots that show the SPDC spectrum for (a) degenerate, copropagating ($\theta=0°$), (b) degenerate, counter-

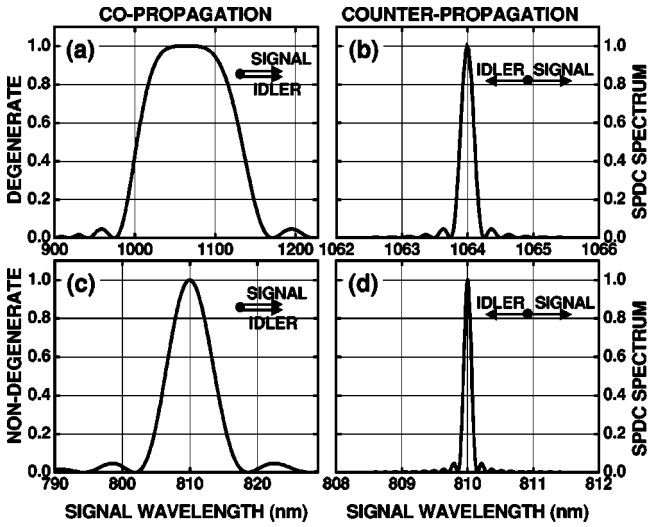

FIG. 6. SPDC spectrum vs signal wavelength λ_s for phase-matching conditions that allow (a) degenerate, copropagating ($\theta=0°$); (b) degenerate, counterpropagating ($\theta=88.2°$); (c) nondegenerate, copropagating ($\Lambda=7.4$ μm, $\theta=0°$); and (d) nondegenerate, counterpropagating ($\theta=69.7°$) signal and idler photons in a PPLN waveguide of 1 mm length. The directions of propagation for the signal and idler photons in the various cases are shown by the insets. Note the different abscissa scales for the copropagating and counterpropagating panels. The full width at half maximum for the copropagating case is 130 nm for degenerate photons versus 7.3 nm for a nondegenerate signal photon at 810 nm. In the counterpropagating case, the FWHM for degenerate photons is 0.23 nm versus 0.13 nm for a nondegenerate signal photon at 810 nm. The poling period in (a), (b), and (d) is $\Lambda=6.8$ μm, whereas for (c) it is $\Lambda=7.4$ μm to achieve a nondegenerate solution for a 0° angle of incidence. The pump wavelength $\lambda_p=532$ nm and the nondegenerate idler photon $\lambda_i=1550$ nm.

propagating ($\theta=88.2°$), (c) nondegenerate, copropagating ($\Lambda=7.4$ μm, $\theta=0°$), and (d) nondegenerate, counterpropagating ($\theta=69.7°$) down-converted photons. In all cases, the PPLN waveguide is taken to have an interaction length $L=1$ mm and a poling period of 6.8 μm (unless otherwise specified), and the pump wavelength is again taken to be 532 nm. It is immediately obvious that the bandwidths for the counterpropagating cases are narrower than those for the copropagating cases [compare Figs. 6(b) and 6(d) with Figs. 6(a) and 6(c)]. This narrow bandwidth arises since the sum, rather than the difference, of the propagation constants appears in the expression for $\Delta\beta'$ [8]. For degenerate signal and idler photons, the reduction in bandwidth from 130 nm for the copropagating case to 0.23 nm in the counterpropagating case is almost three orders of magnitude. This is far in excess of the one order of magnitude reduction in bandwidth available via surface birefringence in a semiconductor waveguide [13]. The pronounced bandwidth reduction in our PPLN structure arises from the strong dispersion of lithium niobate. The narrow bandwidth of the signal and idler supports the approximate discrete-frequency representation provided in Eq. (14) and indicates that nearly discrete down-conversion wavelengths can indeed be realized experimentally without having to resort to the use of narrow spectral filters.

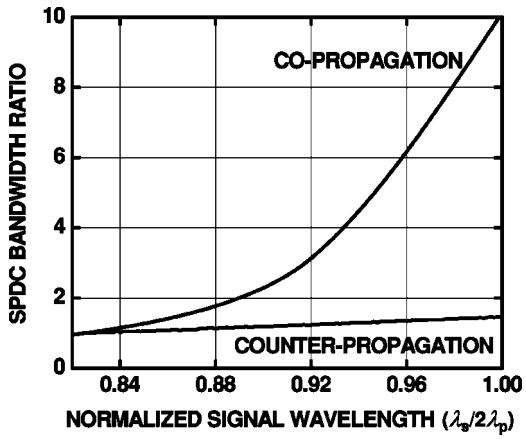

FIG. 7. SPDC bandwidth ratio vs normalized signal wavelength. The bandwidth ratio is obtained by dividing by the bandwidth at $\lambda_s=880$ nm (0.83 on the abscissa), which is the shortest wavelength used for this simulation. The signal wavelength is normalized to the degenerate wavelength $2\lambda_p=1064$ nm. The pump wavelength $\lambda_p=532$ nm. This plot illustrates the relative increase in bandwidth for copropagating and counterpropagating photons as the nonlinear interaction approaches degeneracy at $\lambda_s/2\lambda_p=1.00$.

To highlight the distinction between the copropagating and counterpropagating cases, we present a plot of the SPDC bandwidth ratio versus normalized signal wavelength ($\lambda_s/2\lambda_p$) in Fig. 7. The SPDC bandwidth ratio is obtained by dividing the FWHM bandwidth for each central signal wavelength by the FWHM bandwidth at $\lambda_s=880$ nm, which is the shortest wavelength used for this simulation. The PPLN waveguide is taken to have an interaction length $L=1$ mm and again $\lambda_p=532$ nm. This plot illustrates the relative increase in bandwidth for copropagating and counterpropagating photons as the nonlinear interaction approaches degeneracy ($\lambda_s/2\lambda_p=1.00$). This trend is similar in birefringent phase matching and arises from a change in the refractive index sum or difference for signal and idler photons. The change, however, is much more pronounced for copropagating photons. Note that the bandwidth ratio (and the band-

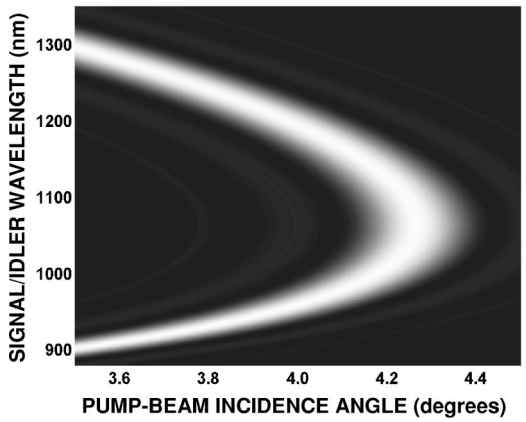

FIG. 8. Spectrum of signal and idler vs pump-beam incidence angle for copropagating beams in a 1-mm PPLN waveguide with a poling period $\Lambda=7.4$ μm and positive grating vector K_m ($m=1$). The pump wavelength $\lambda_p=532$ nm.

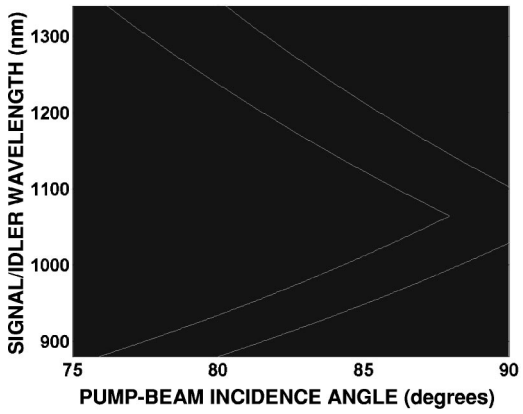

FIG. 9. Spectrum of signal and idler vs pump-beam incidence angle for counterpropagating beams in a 1-mm PPLN waveguide with a poling period $\Lambda = 6.8\ \mu$m and $m = \pm 1$. The pump wavelength $\lambda_p = 532$ nm. The narrow bandwidth of the down-converted light is evident for all signal and idler combinations and does not change appreciably as the photons approach degeneracy, unlike the results shown in Fig. 8 for copropagating beams. Although this plot includes all the information pertaining to the spectrum of the down-converted light, it is visually indistinguishable from the plot presented in Fig. 5(b).

width) of the counterpropagating photons is always less than that for copropagating photons and changes far less as the signal-idler wavelength combination changes.

Just as we did for the analysis presented in Sec. III, we generate tuning curves that illustrate all possible signal-idler combinations for various pump-beam incidence angles. Figure 8 shows the tuning curve obtained for copropagating signal and idler photons in a 1-mm PPLN waveguide when the spectral distribution of the down-converted light is incorporated in the model. To generate such a curve for copropagating photons, it is necessary to increase the poling period in the simulation to 7.4 μm so that nondegenerate solutions can be found as the pump-beam incidence angle is varied. The grating vector K_m is taken to be positive ($m = 1$) to facilitate comparison with previous work in the field. The plot reveals the large bandwidth near degeneracy (1064 nm) and the spectral characteristics of the down-converted light for all wavelength combinations.

Finally, in Fig. 9, we present a tuning curve for counterpropagating signal and idler photons in a 1-mm PPLN waveguide with a poling period of 6.8 μm. In analogy with the analysis carried out in Sec. III, we consider both the positive and negative spatial components of the grating vector ($m = \pm 1$). The resulting plot is similar to that presented in Fig. 5(b) but now incorporates the spectral distribution of the down-converted light. Since the bandwidth of the down-converted light is narrow for all signal-idler wavelength combinations, and does not change appreciably as the photons approach degeneracy, the curves remain narrow for all pump-beam incidence angles.

V. SPDC IN A CLADDING-PUMPED NONLINEAR FIBER

Copropagating entangled photons generated by spontaneous parametric down-conversion have previously been observed in periodically poled silica fibers (PPSFs) by direct coupling of the pump beam [22]. Although the effective nonlinearity d_{eff} in silica is less than that for lithium niobate, PPSFs offer a longer interaction length L, a higher damage intensity threshold I, and a lower refractive index n so that they achieve a comparable figure of merit $d_{\text{eff}}^2 L^2 I / n^3$. The shortest poling period currently available in a D-shaped silica fiber is $\Lambda = 25\ \mu$m, which was used for second-harmonic generation at 422 nm with an average conversion efficiency of $\sim 0.22\%$ [23]. It is expected that this efficiency would be able to be increased by a factor of 100 by improvements in poling techniques.

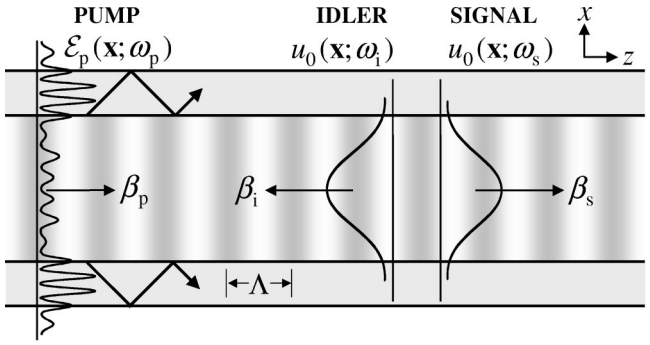

FIG. 10. Meridional cross section of an optical fiber with a periodically modulated nonlinear medium $\chi^{(2)}$ that comprises the core. The pump beam is guided within the fiber cladding. By coupling to the core, spontaneous parametric down-conversion yields counterpropagating signal and idler photons.

As an alternative to the periodically poled silica fiber and to the PPLN waveguide example presented in Secs. III and IV, we present a configuration in which we propose the use of a periodically poled nonlinear optical fiber to generate counterpropagating signal and idler photons. In a scheme analogous to that of a fiber laser, the pump beam (which is guided in the fiber cladding) couples to the core medium as it propagates. Since the core medium has a modulated nonlinearity, as depicted in Fig. 10, counterpropagating entangled photons can be generated. With improvement in the conversion efficiency, the use of cladding-pumped nonlinear fibers such as described above should prove an effective source of counterpropagating entangled photons for quantum-optics experiments and technologies.

VI. CONCLUSION

In Sec. II, we discussed the conditions for achieving spontaneous parametric down-conversion in a waveguide with periodic nonlinearity. We extended this discussion in Sec. III and found that an unguided pump beam in a periodically poled lithium niobate waveguide could give rise to counterpropagating signal and idler photons. In Sec. IV, we considered a particular waveguide structure and computed the spectrum of the down-converted light for several interesting and important cases. The theoretical results indicate that counterpropagating beams have a narrower bandwidth than copropagating beams, which makes it possible to generate a superposition of two or more counterpropagating nondegenerate

photon pairs. The quantum state generated thereby exhibits *discrete* frequency entanglement and can be readily altered in several ways: by tuning the pump-beam incidence angle, by appropriately changing the pump field profile using, e.g., a superposition of pump angles, and by engineering the periodicity of the nonlinearity. Such a quantum state cannot be generated in bulk nonlinear media, nor in media with periodic structures, but they are generated naturally in media with both periodic nonlinearity and a waveguiding structure. Although we primarily discussed theoretical results for a PPLN waveguide, the results are general and will also apply, for example, to a periodically poled cladding-pumped fiber with $\chi^{(2)}$ nonlinearity. Many other configurations for the generation of counterpropagating signal and idler photons can be envisioned.

It may also be possible to admix other levels of subtlety into the quantum states described in this paper. By carefully selecting an appropriate nonlinear medium and crystal cut axes, for example, polarization entanglement can be incorporated into the down-converted photons. It has been shown in potassium titanyl phosphate (KTP) that it is possible to create type-II second harmonic conversion by use of the d_{24} nonlinear coefficient for *z*-cut crystals with the beam propagation along the *x* axis [24]. Further studies along these lines will certainly reveal other such interesting materials, implementations, and devices.

ACKNOWLEDGMENTS

This work was supported by the National Science Foundation; the Center for Subsurface Sensing and Imaging Systems (CenSSIS), an NSF Engineering Research Center; the Defense Advanced Research Projects Agency (DARPA); and the David and Lucile Packard Foundation.

[1] J.A. Giordmaine, Phys. Rev. Lett. **8**, 19 (1962).
[2] P.D. Maker, R.W. Terhune, M. Nisenoff, and C.M. Savage, Phys. Rev. Lett. **8**, 21 (1962).
[3] Y. R. Shen, *The Principles of Nonlinear Optics* (Wiley, New York, 1984), Chaps. 3, 7, and 9.
[4] J.A. Armstrong, N. Bloembergen, J. Ducuing, and P.S. Pershan, Phys. Rev. **127**, 1918 (1962).
[5] P.A. Franken and J.F. Ward, Rev. Mod. Phys. **35**, 23 (1963).
[6] P. Baldi, P. Aschieri, S. Nouh, M.D. Micheli, D.B. Ostrowsky, D. Delacourt, and M. Papuchon, IEEE J. Quantum Electron. **31**, 997 (1995).
[7] L.E. Myers, R.C. Eckardt, M.M. Fejer, R.L. Byer, W.R. Bosenberg, and J.W. Pierce, J. Opt. Soc. Am. B **12**, 2102 (1995).
[8] M.M. Fejer, G.A. Magel, D.H. Jundt, and R.L. Byer, IEEE J. Quantum Electron. **28**, 2631 (1992).
[9] S. Tanzilli, H.D. Riedmatten, W. Tittel, H. Zbinden, P. Baldi, M.D. Micheli, D.B. Ostrowsky, and N. Gisin, Electron. Lett. **37**, 26 (2001).
[10] J. Peřina, Z. Hradil, and B. Jurčo, *Quantum Optics and Fundamentals of Physics* (Kluwer, Boston, 1994), Chaps. 7 and 8.
[11] L. Mandel and E. Wolf, *Optical Coherence and Quantum Optics* (Cambridge University Press, Cambridge, 1995), Chap. 22.
[12] K. Banaszek, A.B. U'Ren, and I.A. Walmsley, Opt. Lett. **26**, 1367 (2001).
[13] A.D. Rossi and V. Berger, Phys. Rev. Lett. **88**, 043901 (2002).
[14] M. Atatüre, G. Di Giuseppe, M.D. Shaw, B.E.A. Saleh, A.V. Sergienko, and M.C. Teich, Phys. Rev. A (to be published).
[15] D. N. Klyshko, *Photons and Nonlinear Optics* (Nauka, Moscow, 1980), Chaps. 1 and 6 (translation, Gordon and Breach, New York, 1988).
[16] G. Di Giuseppe, M. Atatüre, M.D. Shaw, A.V. Sergienko, B.E.A. Saleh, and M.C. Teich, Phys. Rev. A **66**, 013801 (2002).
[17] B. E. A. Saleh and M. C. Teich, *Fundamentals of Photonics* (Wiley, New York, 1991), Chap. 7.
[18] V. G. Dmitriev, G. G. Gurzadyan, and D. N. Nikogosyan, *The Handbook of Nonlinear Optical Crystals*, Springer Series in Optical Sciences Vol. 64, 2nd ed. (Springer-Verlag, New York, 1995), Chap. 3.
[19] R.G. Batchko, M.M. Fejer, R.L. Byer, D. Woll, R. Wallenstein, V.Y. Shur, and L. Erman, Opt. Lett. **24**, 1293 (1999).
[20] Y.J. Ding, S.J. Lee, and J.B. Khurgin, Phys. Rev. Lett. **75**, 429 (1995).
[21] A. Ghatak and K. Thyagarajan, *Introduction to Fiber Optics* (Cambridge University Press, New York, 1998), Chap. 7.
[22] G. Bonfrate, V. Pruneri, P.G. Kazansky, P. Tapster, and J.G. Rarity, Appl. Phys. Lett. **16**, 2356 (1999).
[23] P.G. Kazansky and V. Pruneri, J. Opt. Soc. Am. B **14**, 3170 (1997).
[24] S. Wang, V. Pasiskevicius, J. Hellström, F. Laurell, and H. Karlsson, Opt. Lett. **24**, 978 (1999).